EINDHOVEN
UNIVERSITY OF
TECHNOLOGY

Effect of an electric field during the deposition of silicon dioxide thin films by plasma enhanced atomic layer deposition

Citation for published version (APA):
Beladiya, V., Becker, M., Faraz, T., Kessels, W. M. M., Schenk, P., Otto, F., Fritz, T., Gruenewald, M., Helbing, C., Jandt, K. D., Tünnermann, A., Sierka, M., & Szeghalmi, A. (2020). Effect of an electric field during the deposition of silicon dioxide thin films by plasma enhanced atomic layer deposition: an experimental and computational study. *Nanoscale*, *12*(3), 2089-2102. https://doi.org/10.1039/c9nr07202k

Document license:
TAVERNE

DOI:
10.1039/c9nr07202k

Document status and date:
Published: 21/01/2020

Document Version:
Publisher's PDF, also known as Version of Record (includes final page, issue and volume numbers)

Please check the document version of this publication:

• A submitted manuscript is the version of the article upon submission and before peer-review. There can be important differences between the submitted version and the official published version of record. People interested in the research are advised to contact the author for the final version of the publication, or visit the DOI to the publisher's website.
• The final author version and the galley proof are versions of the publication after peer review.
• The final published version features the final layout of the paper including the volume, issue and page numbers.

Link to publication

General rights
Copyright and moral rights for the publications made accessible in the public portal are retained by the authors and/or other copyright owners and it is a condition of accessing publications that users recognise and abide by the legal requirements associated with these rights.

• Users may download and print one copy of any publication from the public portal for the purpose of private study or research.
• You may not further distribute the material or use it for any profit-making activity or commercial gain
• You may freely distribute the URL identifying the publication in the public portal.

If the publication is distributed under the terms of Article 25fa of the Dutch Copyright Act, indicated by the "Taverne" license above, please follow below link for the End User Agreement:

www.tue.nl/taverne

Take down policy
If you believe that this document breaches copyright please contact us at:

openaccess@tue.nl

providing details and we will investigate your claim.

Download date: 17. Nov. 2023

Published on 19 December 2019. Downloaded by Eindhoven University of Technology on 2/12/2020 12:29:42 PM.

Nanoscale

ROYAL SOCIETY OF CHEMISTRY

PAPER

View Article Online
View Journal | View Issue

Cite this: *Nanoscale*, 2020, **12**, 2089

Effect of an electric field during the deposition of silicon dioxide thin films by plasma enhanced atomic layer deposition: an experimental and computational study†

Vivek Beladiya,[a] Martin Becker,[b] Tahsin Faraz,[c] W. M. M. (Erwin) Kessels,[c] Paul Schenk,[a,d] Felix Otto,[e] Torsten Fritz,[e] Marco Gruenewald,[e] Christian Helbing,[f] Klaus D. Jandt,[f] Andreas Tünnermann,[a,d] Marek Sierka *[b] and Adriana Szeghalmi *[a,d]

The growth, chemical, structural, mechanical, and optical properties of oxide thin films deposited by plasma enhanced atomic layer deposition (PEALD) are strongly influenced by the average-bias voltage applied during the reaction step of surface functional groups with oxygen plasma species. Here, this effect is investigated thoroughly for SiO_2 deposited in two different PEALD tools at average-bias voltages up to −300 V. Already at a very low average-bias voltage (< −10 V), the SiO_2 films have significantly lower water content than films grown without biasing together with the formation of denser films having a higher refractive index and nearly stoichiometric composition. Substrate biasing during PEALD also enables control of mechanical stress. The experimental findings are supported by density functional theory and atomistic simulations. They demonstrate that the application of an electric field during the plasma step results in an increased energy transfer between energetic ions and the surface, directly influencing relevant surface reactions. Applying an electric field during the PEALD process leads to SiO_2 thin films with significantly improved properties comparable to films grown by ion beam sputtering.

Received 21st August 2019,
Accepted 13th December 2019

DOI: 10.1039/c9nr07202k

rsc.li/nanoscale

Introduction

Silicon dioxide (SiO_2) is a widely used dielectric material in integrated circuits and microelectronic devices owing to its relatively low dielectric constant, a large band gap, and a low defect density at the SiO_2/Si interface.[1–3] Additionally, SiO_2 thin films are frequently used in optical coatings as the low refractive index layer in combination with other high refractive index layers for example in antireflection coatings, dichroic mirrors (DCIM), bandpass filters and polarizers.[3–9] Silica thin films are also used as barrier coatings for polymers or as a surface passivation layer for solar cells.[10,11] For optimal performance in these applications, the optical, mechanical, chemical, and structural properties of SiO_2 thin films must be precisely controlled. These properties significantly depend on the deposition method and associated conditions such as the temperature, pressure, reactive species, *etc*. Hence, the relationship between deposition conditions and the film properties warrant thorough investigation.

Advancements in nanotechnology and shrinking device sizes set a stringent requirement on thickness conformality and uniformity of SiO_2 coatings. Precise thickness control of SiO_2 thin films on the atomic scale with conventional thin film deposition techniques, such as physical vapour deposition (PVD) and chemical vapour deposition (CVD) is challenging. Hence, continuous development of deposition technologies is necessary to keep pace with the rapidly increasing demands imposed on ultra-thin films.

Atomic layer deposition (ALD) offers unique advantages in coating large area substrates with good uniformity and 3D sub-

[a]*Institute of Applied Physics, Friedrich Schiller University Jena, Albert-Einstein-Str. 15, 07745 Jena, Germany*
[b]*Otto Schott Institute of Materials Research, Friedrich Schiller University Jena, Fraunhoferstr. 6, 07743 Jena, Germany*
[c]*Department of Applied Physics, University of Technology Eindhoven, P.O. Box 513, 5600MB Eindhoven, The Netherlands*
[d]*Fraunhofer Institute for Applied Optics and Precision Engineering IOF, Albert-Einstein-Str. 7, 07745 Jena, Germany*
[e]*Institute of Solid State Physics, Friedrich Schiller University Jena, Helmholtzweg 5, 07743 Jena, Germany*
[f]*Chair of Materials Science (CMS), Otto Schott Institute of Materials Research, Friedrich Schiller University Jena, Löbdergraben 32, 07743 Jena, Germany*
†Electronic supplementary information (ESI) available. See DOI: 10.1039/c9nr07202k

Published on 19 December 2019. Downloaded by Eindhoven University of Technology on 2/12/2020 12:29:42 PM.

strates with good conformality owing to the self-limiting nature of ALD.[12–16] The sequential and self-limiting surface reactions during ALD enable to Ångstrom level growth control in each ALD cycle.

In conventional thermal ALD, surface reactions are thermally activated by heating the substrate to elevated temperatures. In contrast, plasma enhanced atomic layer deposition (PEALD) allows for low-temperature deposition of thin films owing to the formation of highly reactive radical species in the plasma exposure step.[17–20] However, various other species generated during the plasma exposure, such as ions and photons, may also influence the properties of the film. The energy of ions impinging on a growing film during PEALD can be controlled by implementing external substrate biasing in the plasma exposure step. Controlling ion energy by substrate biasing during PEALD has been shown to enable control over the resulting film properties owing to various ion-induced effects.[21–26] These are known from PVD techniques to include ad-atom migration, desorption, sputtering, displacement of lattice atoms, implantation, and increased sticking coefficient, depending on the ion energies.[27–33] As a result of such ion-induced effects, a wide range of thin film properties such as the crystallinity, growth rate, density, stoichiometry, optical losses, incorporation of –OH groups, refractive index, and mechanical stress can be tailored for serving the desired application.[34–37]

Ion-induced effects during deposition of SiO_2 thin films have extensively been studied in PVD[31,33,38–40] and CVD[2,3,33,41–49] processes. However, oxides deposited by PEALD have a fundamentally different growth mechanism. During PEALD of oxide thin films, organometallic precursor molecules and radicals from oxygen plasma sequentially react with surface functional groups. These surface functional groups can also vary due to the variation in deposition temperature or type of precursor used during PEALD of SiO_2, which can further lead to a variation in the material properties.[17,20,50–52] Hence, the chemical reactions at the surface will determine the surface groups and the material properties.

The surface chemical reactions/functional groups are also highly sensitive to the oxygen ions impinging on the surface of the growing film. We have recently reported the first observations during the PEALD of SiO_2 grown with substrate biasing.[24] However, the influence of substrate biasing on the composition and properties of SiO_2 thin films grown with PEALD requires in depth investigation. Here, we follow up on our previous study by extending the technological basis using a second PEALD system with substrate biasing. We provide insight into the effects of substrate biasing during PEALD of SiO_2 by investigating their chemical composition, chemical resistance, surface morphology, mechanical stress, and optical properties. The experimental results show that very low average-bias voltages are sufficient to alter the surface reactions and surface functional groups in the SiO_2 PEALD process. Finally, the observed trends in the material properties of deposited thin films are clarified through quantum mechanical and atomistic simulations of the SiO_2 PEALD growth process.

Experimental

The SiO_2 thin films were deposited by PEALD using two different reactor configurations. The FlexAL reactor (Oxford Instruments Plasma Technology, Yatton, UK) is configured with a remote inductively coupled plasma (ICP) generator with a power of 600 W at 13.56 MHz radio frequency (RF). Additionally, a 13.56 MHz RF generator is connected to the substrate table through an automatic matching unit (AMU). With this generator average-bias voltages up to −350 V (at ∼1.2 Pa operating pressure) during the plasma exposure can be obtained when supplying up to 100 W power. A grounded substrate corresponds to an average-bias voltage of 0 V. Additional details of the reactor configuration are described elsewhere.[24]

The second reactor is a SILAYO inductively coupled plasma PEALD tool (Sentech Instruments GmbH, Berlin, Germany). This tool is a prototype PEALD tool with a planar triple spiral antenna inductively coupled plasma (PTSA-ICP) source (500 W, 13.56 MHz RF plasma generator). It is the first time that thin film deposition with this tool is being reported and a schematic of the tool is shown in Fig. 1. Substrates of sizes up to 330 mm in diameter and 150 mm height can be handled using this equipment. Additionally, an average-bias voltage up to −250 V (at 2.9 Pa operating pressure) can be applied during the thin film growth using a 500 W 13.56 MHz RF plasma generator controlled by the AMU.

The SiO_2 films (∼200 nm thickness) were deposited in both tools using the BDEAS (bis(diethylamino)silane) precursor and oxygen plasma.[17] The substrates were kept at 200 °C using the FlexAL tool and at 100 °C using the SILAYO tool during the deposition. The films were typically deposited on double-side polished 75 mm diameter c-Si (100) substrates with a thin native oxide of a thickness of about 1.5 nm. To investigate the optical properties, films were also deposited on glass (fused silica and BK7) substrates. The process conditions during SiO_2 deposition with both tools are summarized in Table 1. For films deposited using the FlexAL tool, the precursor pulse and precursor purge times were 0.175 s and 3 s, respectively. Additionally, an extra precursor hold step of 1 s was provided

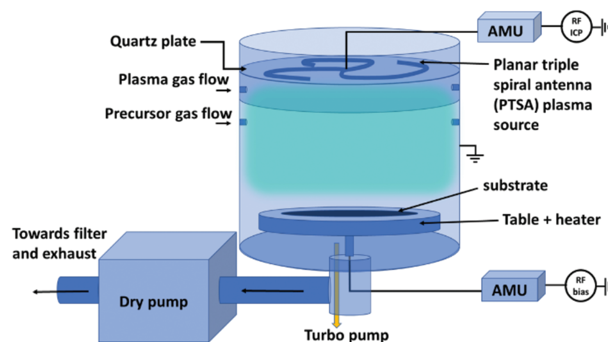

Fig. 1 Schematic of the SILAYO tool. The tool consists of an automatic matching unit (AMU), a radio frequency inductively coupled plasma (RF-ICP) source, a radio frequency bias (RF bias) source, an AMU for substrate biasing.

 This journal is © The Royal Society of Chemistry 2020

Published on 19 December 2019. Downloaded by Eindhoven University of Technology on 2/12/2020 12:29:42 PM.

Table 1 Deposition conditions of SiO_2 thin films

Process parameters	FlexAL	SILAYO
Precursor	BDEAS	BDEAS
Precursor temperature	50 °C	50 °C
Precursor delivery type	Direct draw	Bubbler mode
Deposition temperature	200 °C	100 °C
ICP power	200 W	100 W
O_2 flow	100 sccm	200 sccm
Ar flow	—	30 sccm
Operating pressure	2 Pa	3 Pa
BDEAS pulse	0.175 s	0.320 s
Precursor hold	1 s	—
Precursor purge	3 s	5 s
Plasma pulse (additionally substrate biasing)	5 s (substrate biasing was applied during complete 5 s of plasma pulse)	3 s (substrate biasing was applied during complete 3s of plasma pulse)
Plasma purge	2 s	2 s

after the precursor pulse step to ensure sufficient time for the precursor reaction. Furthermore, during the plasma step, substrates were exposed to an oxygen plasma for 5 s using an O_2 gas flow of 100 sccm. The average-bias voltage up to −295 V (see Table 2) was applied during the full 5 s of the plasma exposure step, followed by 2 s of plasma purge.

For films deposited using the SILAYO tool, the precursor was pulsed for 0.320 s followed by 5 s of precursor purge. Subsequently, the oxygen plasma pulse was introduced for 3 s using a mixture of O_2 (200 sccm flow) and Ar (30 sccm flow). An average-bias voltage up to −100 V (see Table 2) was applied during the full 3 s of the oxygen plasma exposure step. This was followed by 2 s purge of the reaction by-products and residual gas species. Thin films without bias were deposited for the purpose of comparison. Additionally, SiO_2 thin films without bias were deposited with a capping layer of Al_2O_3 with 30 nm thickness. This has been done to investigate the environmental influence on the SiO_2 composition and properties, which might be influenced by moisture when the samples are exposed to air.

The growth per cycle (GPC), thickness, and optical constants of SiO_2 films deposited using the FlexAL tool were determined by spectroscopic ellipsometry (M2000D, J. A. Woollam Co., Inc., Lincoln, NE) using a rotating compensator ellipsometer (190–1000 nm). The model consisting of the silicon substrate, a native oxide (~1.5 nm), and a silicon dioxide layer was fitted using a Cauchy dispersion relation. The data were fitted in the wavelength range from 200–1000 nm. The thickness and optical constant of the SiO_2 films deposited using the SILAYO tool were determined using an 850 spectroscopic ellipsometer (Sentech Instruments GmbH, Berlin, Germany). The model used for fitting these films was similar to the one mentioned above and the wavelength range was 200–980 nm. The coating non-uniformity of the SiO_2 films deposited using the SILAYO tool was mapped (69 points) on 200 mm c-Si substrates. The SILAYO tool generates a homogeneous plasma due to the PTSA plasma source and thus enables uniform thin film growth with non-uniformity below 1% on 200 mm substrates and conformal coatings on 3D substrates.

Table 2 Applied RF power on the substrate during the oxygen plasma step and the resulting average-bias voltage

Applied RF power (W)	Obtained average-bias voltage (V)	Applied RF power (W) (automatic)	Obtained average-bias voltage (V)
FlexAL	FlexAL	SILAYO	SILAYO
0	0	—	0
10	−111	25–80	−1
50	−206	200–300	−5
95	−295	200–350	−10
		150–400	−20
		200–400	−30
		200–450	−50
		350–500	−100

X-ray reflectivity (XRR) analysis was performed using a Bruker-AXS D8 advanced system (Bruker Corporation, Billerica, MA, USA) in the grazing incidence configuration with a Cu Kα X-ray source (radiation wavelength 0.154 nm) to investigate thickness, density, and surface roughness of the SiO_2 thin films. The same system was also used to perform X-ray diffraction (XRD) measurements.

In addition to XRR, the root mean square (RMS) surface roughness of the SiO_2 films was determined using atomic force microscopy (AFM). The AFM measurements were performed on films deposited on c-Si and glass substrates using a Dimension 3100 (Bruker Corporation, Billerica, MA, USA) equipped with a Nanoscope IV controller at ambient temperature in air. Standard cantilevers from Bruker (model RTESP, Santa Barbara, CA, USA) featuring a resonance frequency in the range of 315–364 kHz in air, a spring constant in the range of 20–80 N m^{-1}, and a typical tip radius of less than 10 nm were used. The sample area of 2 μm × 2 μm was scanned in tapping mode.

The mechanical stress of the deposited SiO_2 thin films was determined from wafer curvature measurements (FLX-2320, KLA-Tencor, San Jose, USA). The wafer curvature of the Si wafer of 75 mm diameter and ~400 μm thickness was measured before and after the deposition to determine residual stress. The residual stress (σ) in the film was then calculated using Stoney's equation (eqn (1)):

$$\sigma = \frac{1}{6}\frac{E_s}{(1-\vartheta_s)}\left(\frac{1}{R_f}-\frac{1}{R_s}\right)\frac{{t_s}^2}{t_f} \tag{1}$$

where E_s is the Young's modulus, ϑ_s is the Poisson's ratio of the substrate, R_s and R_f are the radii of curvature of the substrate before and after coating, and t_s and t_f are the thickness of the substrate and the film, respectively. We note that positive and negative sign of the stress values denotes tensile and compressive stress, respectively.

The chemical composition of the film was analysed using a Fourier transform infrared spectroscopy (FTIR) system (Varian Inc., Palo Alto, CA, USA). FTIR measurements were performed in the wavenumber range from 400 to 4000 cm^{-1}.

This journal is © The Royal Society of Chemistry 2020

Published on 19 December 2019. Downloaded by Eindhoven University of Technology on 2/12/2020 12:29:42 PM.

The film composition was analyzed using X-ray photoelectron spectroscopy (XPS, XR 50 M X-ray source with FOCUS 500 monochromator, SPECS Surface Nano Analysis GmbH, Berlin, Germany) using Mg Kα radiation (1253.6 eV) in normal emission. The high-resolution spectra were fitted using OriginPro2017. The fitting details are provided in the ESI.†

Auger electron spectroscopy (AES, Varian Inc., Palo Alto, CA, USA) depth profiling was also performed using an Auger cylindrical mirror spectrometer. The electron beam of 5 keV was focused on the samples at 30° angle of incidence, and the films were sputtered using krypton (Kr) ions at 2 keV energy and 10 μA current. The base pressure for the XPS and the AES equipment was 2×10^{-10} mbar. The pump down time for a pressure below 1×10^{-6} mbar for the XPS equipment was 2 h, and 10 h for the AES equipment, respectively.

The optical loss of SiO_2 thin films deposited on fused silica and BK7 substrates were calculated from transmittance (T)/reflectance (R) spectra ($100 - T - R$%) measured using a Lambda 900 spectrophotometer from PerkinElmer Inc. (Waltham, MA, USA).

To investigate the chemical stability, SiO_2 films were immersed in 85% H_3PO_4 for 1 h, 1 day, 4 days, 5 days, and 7 days as well as in 1 M NaOH solution for 1, 2, 4, and 24 h at room temperature. After etching, the samples were rinsed in a solution containing water–isopropanol mixture, followed by rinsing in water. Finally, the samples were dried using N_2 gas.

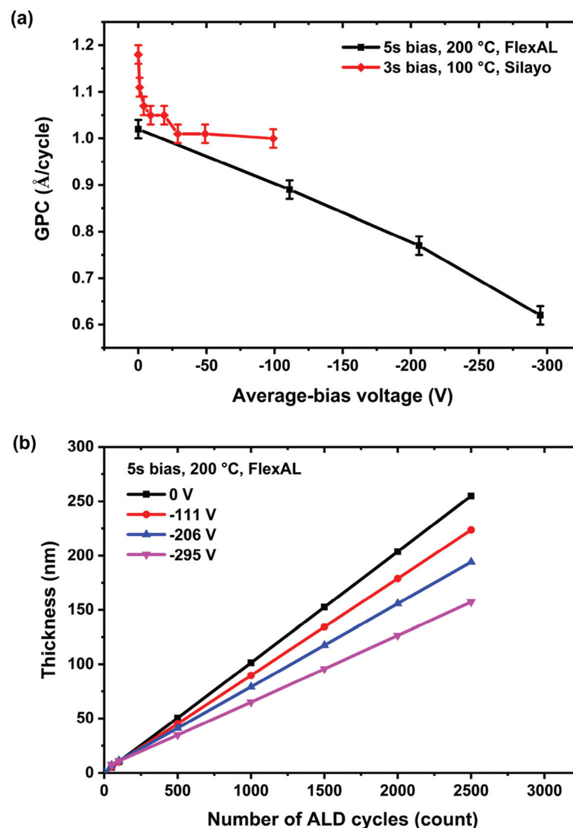

Fig. 2 (a) Variation in the growth per cycle (GPC) of SiO_2 thin films (using the FlexAL and the SILAYO tools) as a function of average-bias voltage measured *ex situ* using spectroscopic ellipsometry and (b) thickness evolution with the number of ALD cycles (FlexAL) measured *in situ* by using spectroscopic ellipsometry.

Computational

For all density functional theory (DFT) calculations the TURBOMOLE program package[53,54] was used, along with the Perdew–Burke–Ernzerhof (PBE) exchange–correlation functional[55] and def2-TZVP basis sets.[56] The Grimme dispersion correction (DFT-D3) was added to account for the dispersion forces.[57,58] PEALD layer growth simulations used the protocol combining Monte Carlo (MC) deposition algorithm and structure relaxation using molecular dynamics (MD), as described in details in ref. 59. The Atomic Simulation Environment (ASE)[60] was employed for storing and manipulating structure models as well as for reading and writing of all input and output files. Structure relaxation and MD simulation used the General Utility Lattice Program (GULP)[61] and the ReaxFF reactive force field[62] with parameters taken from the literature.[62–64]

Results and discussion

Film growth

The growth per cycle (GPC) of the SiO_2 films was calculated from the thickness measured *via* spectroscopic ellipsometry. The GPC of the film deposited using the FlexAL tool without bias was 1.02 Å per cycle (Fig. 2a) which is similar to the GPCs reported in the literature for SiO_2 PEALD with the same precursor and with various tools.[20,50,65] This GPC is similar to the GPC of 0.98 Å per cycle using tris(dimethylamino)silane (3DMAS), and significantly lower than 1.85 Å per cycle reported for the AP-LTO 330® precursor.[50] Fig. 2b shows the *in situ* film thickness growth *versus* the number of cycles of SiO_2 films deposited using the FlexAL tool. The film thickness increases linearly with the number of cycles. *In situ* measurements of the GPC yield results similar to *ex situ* measurements.

On applying substrate bias during the oxygen plasma step in the FlexAL tool, the GPC decreased linearly from 1.02 to 0.62 Å per cycle on increasing average-bias voltage from 0 V to −295 V (Fig. 2a). A similar behaviour was observed for films deposited with substrate biasing using the SILAYO tool. The GPC of the film deposited without bias was 1.18 Å per cycle which decreased to 1.00 Å per cycle on increasing average-bias voltage to −100 V. A rapid decrease of the GPC was observed using the SILAYO tool on applying substrate biasing. The GPC decreases to approximately 1.05 Å per cycle when the average-bias voltage of −20 V was applied and remains nearly constant with a further increase of the average-bias voltage. This change of the GPC suggests significant changes in both the reaction kinetics and the availability of surface functional groups, which will be further analysed in terms of DFT calculations.

This journal is © The Royal Society of Chemistry 2020

Published on 19 December 2019. Downloaded by Eindhoven University of Technology on 2/12/2020 12:29:42 PM.

Structural properties

The density of the SiO_2 thin films determined from XRR measurements are shown in Fig. 3. The SiO_2 film deposited without bias using the FlexAL tool has a density (2.3 ± 0.1 g cm^{-3}) which is similar to previously reported values.[20,66] The SiO_2 film deposited with −295 V average-bias voltage shows a density of 2.4 ± 0.1 g cm^{-3} (Table 3). In the case of the films deposited using the SILAYO tool at 100 °C, the density of the film deposited without bias (Fig. 3) was slightly lower (2.15 ± 0.07 g cm^{-3}) which is similar to the density reported by Dingemans *et al.*[20] The density increases to a maximum value of 2.26 ± 0.07 g cm^{-3} when an average-bias voltage of −1 V was applied. By further increasing the average-bias voltages up to −100 V, the density of SiO_2 films varies within the measurement accuracy and were similar to the densities of films deposited using the FlexAL tool. Applying a low average-bias voltage of −1 V using the SILAYO tool, seems to be sufficient to already induce changes in the film structure. Although the XRR data are rather difficult to assess due to the small changes in density, these observations are confirmed by the refractive index dispersion values obtained as a function of the applied average-bias voltage. These are discussed in the optical properties section.

The increase in density of SiO_2 films with ion-bombardment has been attributed to the reordering of the amorphous SiO_2 network.[67] Hausmann *et al.* and Choi *et al.* have attributed the increase in density to the increased cross-linking rate of Si–O–Si at deposition temperatures higher than 200 °C.[68,69] Hence, it might be possible that for SiO_2 films deposited with substrate biasing, oxygen ions (using the FlexAL tool), and oxygen and argon ions (using the SILAYO tool) bombard the surface and transfer energy in the form of localized heating (thermal spike),[70,71] thereby favouring higher cross-linking rates. Therefore, the increase in cross-linking of Si–O–Si can result in an increase in density (at −295 V using the FlexAL tool and at −1 V using the SILAYO tool) and thereby a decrease of GPC with an increase in average-bias voltage.

The surface roughness of the silica films as determined from AFM and XRR measurements show little dependence on the deposition conditions. Fig. 4 shows the 2 × 2 μm^2 AFM images of silica films deposited on the c-Si substrate at 200 °C with and without substrate biasing using the FlexAL tool.

The roughness of silica films deposited on fused silica and BK7 substrates was slightly higher than that on the c-Si substrate indicating the impact of substrate morphology on the growing film (Table 4). However, the roughness of the SiO_2 films deposited on glass substrates (BK7 and fused silica) were similar to the roughness of the uncoated substrates. The SiO_2 films deposited using the FlexAL tool are rather smooth independent of the applied average-bias voltage. Hence, significant surface damage by the ions impinging on the surface can be ruled out. The thin films deposited using the SILAYO tool need to be investigated to assess the effect of the oxygen + argon plasma on possible surface damage. The XRR measurement shows nearly constant roughness of SiO_2 films deposited with and without bias on the c-Si substrate, which is in agree-

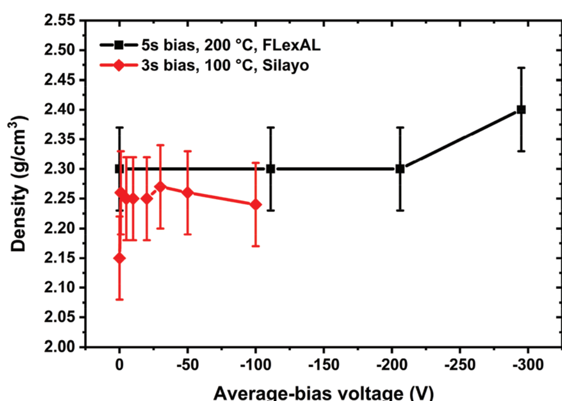

Fig. 3 Variation in the density of SiO_2 thin films deposited using the FlexAL and the SILAYO tools with increasing average-bias voltage measured using XRR.

Table 3 Variation in the growth per cycle, the density, and mechanical stress with average-bias voltage during deposition of SiO_2 thin films using the FlexAL and the SILAYO tool

	Average-bias voltage (V)	GPC[a] (Å per cycle)	ρ^b (g cm^{-3})	Mechanical stress[c] (MPa)
FlexAL	0	1.02	2.3	−76
	−111	0.89	2.3	−253
	−206	0.77	2.3	−225
	−295	0.62	2.4	−246
SILAYO	0	1.18	2.15	1
	−1	1.11	2.26	−271
	−5	1.07	2.25	−221
	−10	1.05	2.25	−190
	−20	1.05	2.25	−184
	−30	1.01	2.27	−185
	−50	1.01	2.26	−164
	−100	1.00	2.24	−137

[a] Growth per cycle (GPC) (±0.02 Å per cycle). [b] Density (SiO_2 − FlexAL ± 0.1 g cm^{-3}, SiO_2 − SILAYO ± 0.07 g cm^{-3}). [c] Mechanical stress (SiO_2 − FlexAL ± 50 MPa, SiO_2 − SILAYO ± 25 MPa).

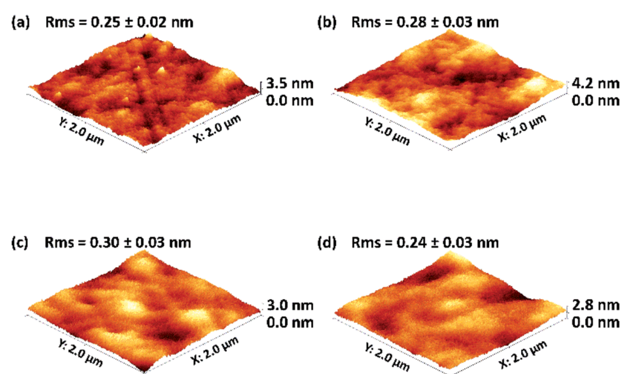

Fig. 4 AFM images of SiO_2 thin films (FlexAL) on applying (a) 0 V (b) −111 V (c) −206 V (d) −295 V average-bias voltage during the oxygen plasma pulse.

Published on 19 December 2019. Downloaded by Eindhoven University of Technology on 2/12/2020 12:29:42 PM.

Table 4 Root mean square (RMS) roughness of SiO_2 thin films deposited on c-Si, fused silica and BK7 substrates when average-bias voltages of 0 V to −295 V were applied during oxygen plasma pulse (FlexAL)

AFM				XRR
Average-bias voltage (V)	c-Si substrate RMS (nm)	Fused silica substrate RMS (nm)	BK7 substrate RMS (nm)	c-Si substrate RMS (nm)
Bare substrate	0.07 ± 0.01	0.32 ± 0.08	0.55 ± 0.07	—
0	0.25 ± 0.02	0.43 ± 0.03	0.50 ± 0.03	1.0 ± 0.1
−111	0.28 ± 0.03	0.29 ± 0.04	0.63 ± 0.03	0.9 ± 0.1
−206	0.30 ± 0.03	0.39 ± 0.03	0.60 ± 0.03	0.9 ± 0.1
−295	0.24 ± 0.03	0.42 ± 0.01	0.50 ± 0.14	1.0 ± 0.1

ment with the trend shown by the AFM measurements. These measurements, therefore, demonstrate that substrate biasing during deposition has no significant effect on the surface roughness of silica films deposited using the FlexAL tool.

Chemical composition

X-ray photoelectron spectroscopy was used to determine the chemical composition of silica films deposited using the FlexAL tool. The O/Si ratio calculated from XPS spectra of the SiO_2 film surface for coatings without substrate biasing using the FlexAL tool is 1.68 ± 0.05 (see Table 5). On increasing average-bias voltage, the XPS spectra of SiO_2 films shows a nearly constant O/Si ratio at the film surface. The peak fitting and O/Si calculation are given in the ESI (Fig. S1–S4†).

Additionally, depth profiling was carried out using Auger electron spectroscopy (AES) to investigate the stoichiometry (O/Si) and impurities in the bulk region of the films (Fig. 5). The O/Si ratio of the SiO_2 film deposited without bias was 1.57, and for the films with −111 V, −206 V and −295 V were 1.53, 1.72 and 1.94, respectively (Table 5). The O/Si ratio at the surface of the SiO_2 films determined using AES (shown in Fig. 5) was around 1.60, 1.34, 1.40 and 1.70 for film deposited with 0 V, −111 V, −206 V and −295 V, respectively. The low O/Si ratio measured by AES at the film surface is in agreement with the low O/Si ratio determined from surface XPS measurement (see Table 5). Ma *et al.* have shown that the densities of SiO_2 films can decrease with an increase in oxygen deficiency. The densities of $SiO_{1.8}$ and $SiO_{1.6}$ were lower than that of the SiO_2 film.[72] Thus, the variation in the density discussed in the previous section correlates with the stoichiometry determined by the AES measurements. The carbon and nitrogen content in the

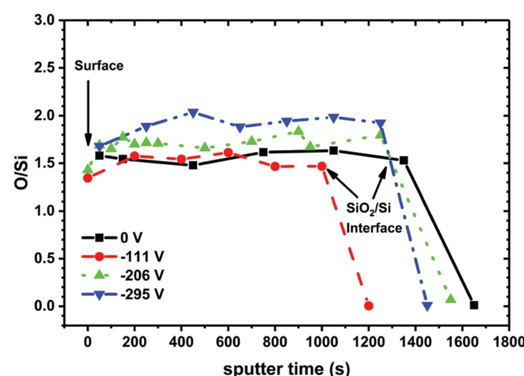

Fig. 5 AES spectra showing variation in the O/Si ratio with an increase in average-bias voltage (SiO_2 films deposited using the FlexAL tool).

film without bias was 0.1% and 0.3%, respectively. The carbon impurities in the film deposited with bias were close to the detection limit, and the standard deviation of the C content is large. The nitrogen content in the films deposited without bias and −111 V bias is also close to the detection limit. On further increase in average-bias voltage, the nitrogen content increased to 1.46% in a film deposited with −295 V average-bias voltage.

To investigate the composition and the –OH content in the films, Fourier transform infrared spectroscopy (FTIR) was performed. Fig. 6a (SiO_2 – FlexAL) and Fig. 6c (SiO_2 – SILAYO) show normalized infrared absorption spectra with three major peaks in the wavenumber range of 450 to 1400 cm^{-1}. The absorption peaks at 460, 810, and 1068 cm^{-1} correspond to Si–O–Si rocking, Si–O–Si bending, and Si–O–Si stretching vibration modes, respectively.[20] The peak at the Si–O–Si stretching mode for SiO_2 film deposited without bias at

Table 5 Effect of substrate biasing on the composition and the refractive index of SiO_2 thin films deposited using the FlexAL tool

Average-bias voltage (V)	XPS[a] (±0.05) O/Si	AES[b] O/Si[b] (±0.06)	AES[b] C[b] (%)	AES[b] N[b] (%)	n^c (±0.003)	Etching rate[d] (nm h^{-1})
0	1.68	1.57	0.11 ± 0.12	0.09 ± 0.08	1.453	1.71
−111	1.61	1.53	0.00 ± 0.00	0.00 ± 0.00	1.469	0.77
−206	1.59	1.72	0.05 ± 0.05	0.36 ± 0.12	1.469	0.74
−295	1.68	1.94	0.02 ± 0.01	1.46 ± 0.71	1.472	0.77

[a] Determined from curve fitting of XPS high-resolution spectra. [b] Determined from Auger electron spectroscopy depth profiling. [c] Refractive index @633 nm. [d] Determined from measuring thickness change of SiO_2 films before and after etching using ellipsometry.

 This journal is © The Royal Society of Chemistry 2020

Published on 19 December 2019. Downloaded by Eindhoven University of Technology on 2/12/2020 12:29:42 PM.

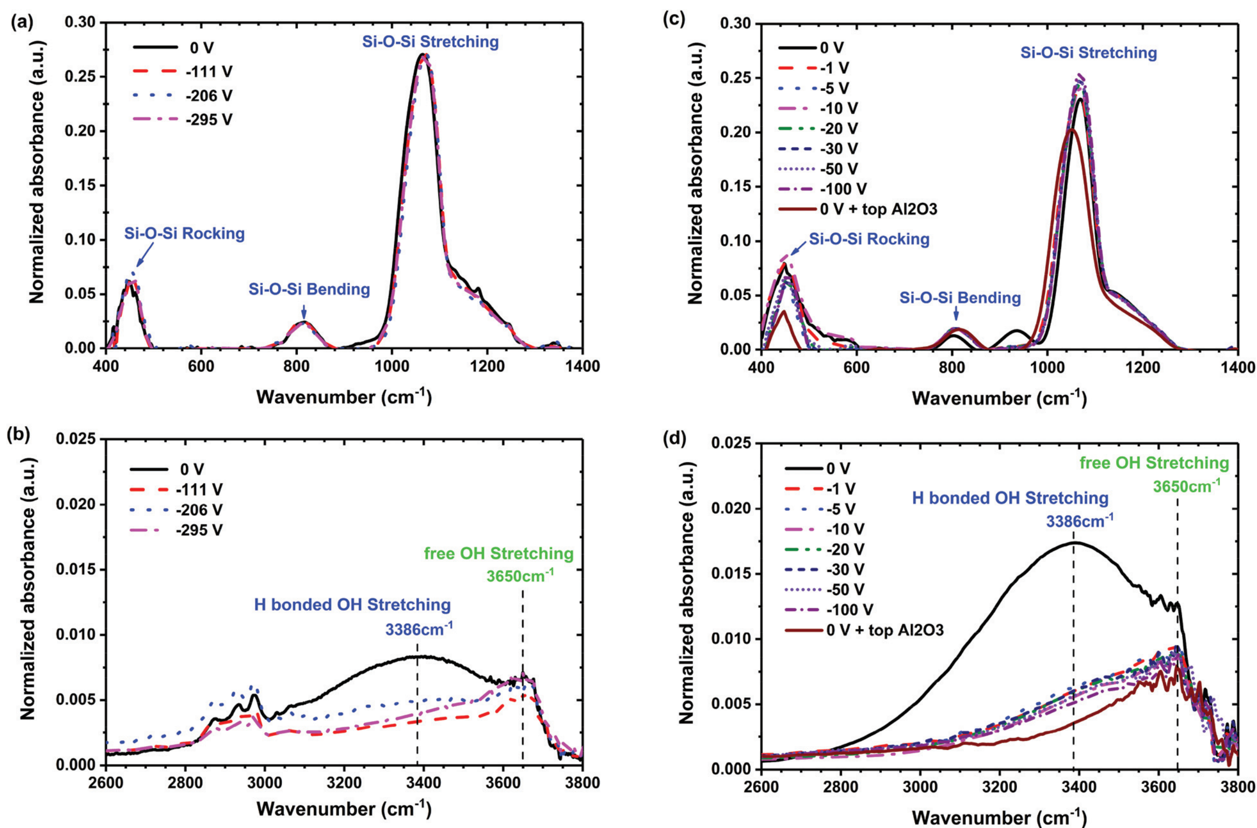

Fig. 6 FTIR spectra of SiO_2 films with different average-bias voltages. Complete absorbance spectra of SiO_2 films deposited with (a) FlexAL and (c) SILAYO tools. The peak corresponding to OH impurities in SiO_2 films deposited by (b) FlexAL and (d) SILAYO tools.

1063 cm^{-1} is slightly shifted to a higher wavenumber of 1071 cm^{-1} in the film grown with −295 V average-bias voltage. The shift to the higher wavenumber can be due to the increase in thickness[43] or a change in stoichiometry as reported by Pai *et al.*[73] The Si–O–Si stretching mode at 1075 cm^{-1} for stoichiometric films shifted to 940 cm^{-1} for off-stoichiometric SiO_x ($x < 2$) films.[73,74] Hence, the FTIR data seem to be in agreement with AES results indicating that the films deposited with the bias are close to stoichiometric SiO_2 compared to SiO_2 film deposited without bias (O/Si = 1.57).

The absorbance spectra (Fig. 6b) between 3100 and 3800 cm^{-1} indicate an OH incorporation in the SiO_2 thin films.[75] The peak around 3650 cm^{-1} corresponds to hydroxyl groups isolated from the neighbouring groups of the SiO_2 network and the broad peak around 3400 cm^{-1} corresponds to hydrogen bonded OH groups.[43] The presence of a peak at 3650 cm^{-1} can be found in all samples because amorphous SiO_2 has a highly distorted Si–O–Si structure and is prone to OH incorporation. The broad peak in the range from 3100–3500 cm^{-1} can be due to OH or adsorbed H_2O incorporated during the deposition or, alternatively, upon removal from the vacuum reactor.[76]

In order to clarify this, a thin capping layer of Al_2O_3 was grown on top of a SiO_2 film grown without bias in the SILAYO tool (see Fig. 6d). The capping layer prevents moisture ingress into the SiO_2 thin film from the environment through open pores in the film.[50] The OH content is proportional to the peak intensity of the OH stretching mode. A significant decrease of the band of the hydrogen bonded OH stretching mode can be observed upon applying an average-bias voltage to the substrate during plasma exposure. Only a weak shoulder at 3386 cm^{-1} is observed for the layer with the capping alumina. This indicates that the hydrogen bonded OH groups observed in the SiO_2 film grown without substrate biasing originate from H_2O adsorbed under ambient conditions and not during the film growth. The thin ALD capping layer is thus efficient in preventing water adsorption into the film.

A drastic change of the OH content is observed for the films grown with an electric field (Fig. 6b and d). Already at −1 V average-bias, the broad peak around 3386 cm^{-1} is reduced. Noteworthy, no capping layer has been applied for the films grown with bias. Clearly, the SiO_2 PEALD layers grown with average-bias voltages applied during oxygen plasma exposure have significantly fewer open pores than the SiO_2 grown without bias. This observation is also supported by vacuum-to-air shift measurements (not shown), whereby the transmittance of the coating on BK7 substrates is measured in a vacuum (10^{-5} mbar) and ambient conditions.[50] While the films grown without substrate biasing have a slight shift of the transmittance maximum due to a change of the effective index

Published on 19 December 2019. Downloaded by Eindhoven University of Technology on 2/12/2020 12:29:42 PM.

when the open pores are filled by H_2O from the air, the films grown with substrate biasing show no shift. The use of substrate biasing prevents the formation of any open pores and increases the density of SiO_2 film during PEALD. The significant decrease in OH impurity on applying average-bias voltages indicates the prominent impact of energetic ions on the Si–O–Si chain by facilitating a denser Si–O bonding environment. The bonding environment is further analysed in terms of atomistic simulations.

Etching test

The chemical stability of the films deposited using the FlexAL tool is further assessed by etching in acid and base solutions. All films were resistant to etching in H_3PO_4 solution (not shown). Ghazaryan *et al.* have shown that phosphoric acid can be used to selectively etch Al_2O_3 from Al_2O_3/SiO_2 mixture to produce nano-porous films without removing SiO_2.[77,78] The NaOH solution, however, has been observed to etch all SiO_2 films.

A significant decrease in the etching rate in a 1 M NaOH solution was observed for films deposited with substrate biasing compared to the film deposited without bias. The film deposited without bias had an etching rate of 1.71 nm h^{-1}, and films deposited with substrate biasing had etching rates around 0.74–0.77 nm h^{-1} (see Table 5).

Seidel *et al.* have reported on the effect of etching SiO_2 in aqueous NaOH, KOH, and LiOH solutions.[79] It was shown that cations (Na^+, K^+, and Li^+) have little effect on etching rates of SiO_2 and that the etching is mainly governed by the OH^- concentration. The effect of RF power and pressure on the etching rates of magnetron sputtering deposited SiO_2 films in 40% KOH at 70 °C solution was investigated by Bhatt *et al.*[80] When studying the influence of pressure for a constant RF power, it was observed that thin films with higher etching rate (chemically less stable) were grown at a higher pressure. With an increase in pressure, the mean free path of the energetic ions impinging on the grown film decreases. This causes those ions to undergo collisions and lose energy before reaching the substrate and thereby yield films with lower density and chemical stability.[81] Hence, a higher etching rate of the SiO_2 film deposited without bias can also be correlated to its lower density, in contrast to the denser and more etch resistant films obtained with substrate biasing. The chemical stability of thin film coatings is highly relevant for various application areas including semiconductors and medical devices, but also optical or photovoltaic applications for components used in the environment.

Mechanical property

Mechanical stress in thin films can cause severe limitations in the performance of devices for advanced applications. High tensile stress can lead to cracking, high compressive stress can cause buckling and delamination of films from the substrate.[82] Hence, it is important to understand its origin. Mechanical stress in the thin film can be extrinsic resulting from the difference in thermal expansion coefficient between the thin films and the substrate, or intrinsic. The intrinsic stress in the films is the product of microstructural evolution in thin films due to grain boundary dislocations, phase transformation, excess vacancies, and formation of voids or incorporation of foreign atom.[82–87] Recently, Abadias *et al.* discussed how limitations due to stress in thin films can be overcome in various application, but the main challenge remains the optimization of thin films with low mechanical stress.[88]

The mechanical stress is compared between the set of coatings deposited with and without substrate biasing at the same deposition temperature. Hence, it can be assumed that the stress difference between films is due to intrinsic effects.

A low residual compressive stress of −96 MPa was observed in silica films deposited without bias using the FlexAL tool (Fig. 7). This value is close to that of the films deposited at 200 °C as observed in the literature.[50,66,89] On applying an average-bias voltage, the residual stress increased and remained roughly constant around −250 MPa.

A similar trend was observed in films deposited using the SILAYO tool. The film deposited without bias had 1 MPa tensile stress. On applying a low bias of −1 V, the compressive stress increased to −287 MPa. An increase in compressive stress with an increase in the energy of species bombarding the SiO_2 film surface has been observed by Simurka *et al.* for films grown by RF magnetron sputtering.[81] The increase in compressive stress in the film deposited with higher ion energies (due to high average-bias voltage) can be attributed to the ion-peening effect and correlates with the increase in density of SiO_2 film deposited with high average-bias voltage (−295 V) using the FlexAL tool and even low average-bias voltage (−1 V) using the SILAYO tool.[70,87] The OH content in the film reduces the oxide viscosity and this results in compressive stress in the films.[90] These effects agree with the observed increase in compressive stress with a decrease in OH incorporation in the PEALD coated SiO_2 films by applying bias as studied in this work (Fig. 6b and d).

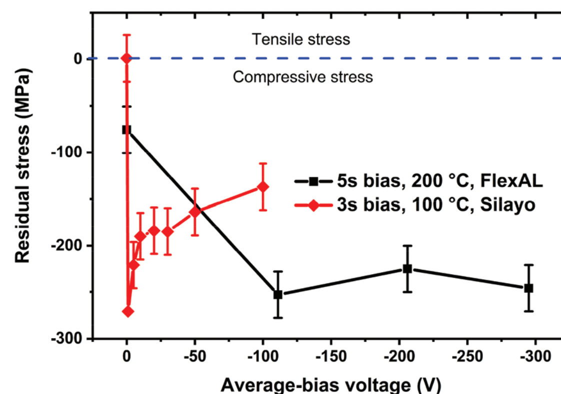

Fig. 7 Mechanical stress *vs.* average-bias voltage of SiO_2 films deposited at 200 °C and 100 °C using the FlexAL and the SILAYO tools, respectively.

 This journal is © The Royal Society of Chemistry 2020

Published on 19 December 2019. Downloaded by Eindhoven University of Technology on 2/12/2020 12:29:42 PM.

Note that the effect of substrate biasing is extremely pronounced for the films grown with the SILAYO tool since very low average-bias voltage values are enough to strongly alter the film stress. The stress in the films decreases on increasing average-bias voltage higher than −1 V. Since the plasma consists a mixture of O_2 + Ar gases during deposition of films using the SILAYO tool, it can be possible that the physical effect of Ar^+ ion bombardment at average-bias voltage higher than −1 V plays a role in stress relaxation and thereby decreasing density.

Optical properties

The increase of the film density of the SiO_2 films grown with average-bias voltage is clearly supported by the increase of the refractive index (Fig. 8a). The refractive index of films grown without bias determined *in situ* in the FlexAL tool is significantly smaller than *ex situ* values measured for films in the environment. When removed from the reactor, the open pores of the SiO_2 films are filled by moisture and the effective refractive index increases. When applying an electric field, the refractive index is significantly higher reaching approximately 1.47 at 633 nm wavelength.

The dispersion curves of the SiO_2 thin films deposited using the FlexAL tool is depicted in Fig. 8b. The refractive index of SiO_2 films deposited with substrate biasing was higher than that of the films deposited without bias. This can be attributed to an increase in density in the films grown with substrate biasing. However, the refractive index of SiO_2 films deposited with increasing average-bias voltage using the FlexAL tool was nearly constant. In comparison, the refractive index increases to the maximum value for the SiO_2 film deposited with an average-bias voltage of −1 V using the SILAYO tool and slightly decreases with increasing average-bias voltage. This suggests further effects to occur at higher ion energies.

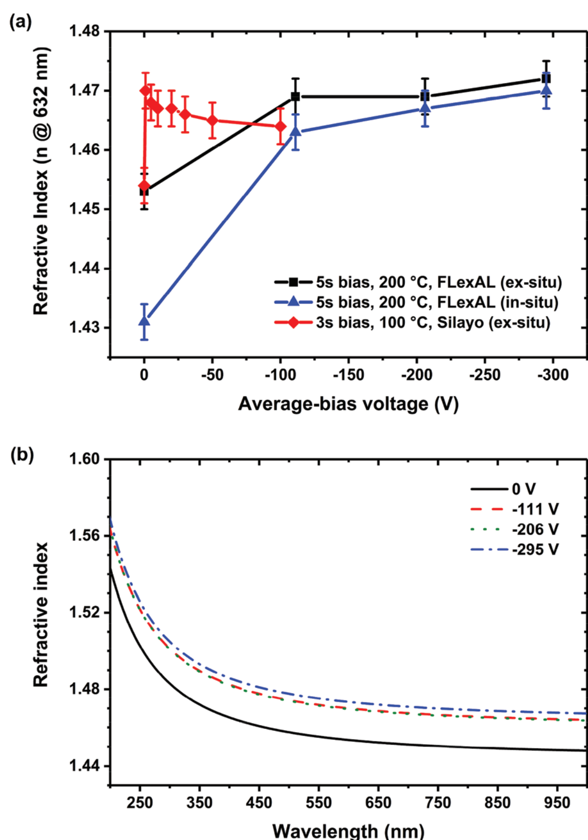

Fig. 8 (a) Refractive index variation with an average-bias voltage of the SiO_2 thin films deposited using the FlexAL and the SILAYO tool (b) dispersion curves of SiO_2 thin films deposited with PEALD with an average-bias voltage up to −295 V using the FlexAL tool.

The refractive index of the SiO_2 film deposited without bias (using both the FlexAL and the SILAYO tools) at 633 nm wavelength is 1.453 ± 0.003.[20,50] The SiO_2 films deposited with substrate biasing had higher refractive index of 1.472 ± 0.003 for films deposited using the FlexAL tool. The refractive index of a SiO_2 film deposited with −1 V using the SILAYO tool reached a maximum at 1.470 ± 0.003 which decreased slightly to 1.464 ± 0.003 when an average-bias voltage of −100 V was applied. Refractive indices of most SiO_2 thin films at 550 nm wavelength are around 1.45. Lee *et al.*[91] reported a refractive index of 1.47 for PEALD SiO_2 films deposited using DIPAS (di(isopropylamino)-silane) and O_2 plasma. These results correlate well with observations in PEALD[20,50] and PVD[75] grown SiO_2 thin films.

Typically, high refractive indices ($n > 1.48$) and dense films ($\rho > 2.3$ g cm^{-3}) can be obtained for SiO_2 deposited by ion beam sputter deposition (IBSD).[92] For these films, the refractive index depends also on the gas type used for the bombardment (Ar or Xe) and on the properties of the impinging species (*e.g.* ion energy and ion incidence angle). In the case of plasma ion-assisted deposition (PIAD) of evaporated SiO_2, the refractive index is around 1.45 for the film deposited by applying −80 V bias voltage, whereby the refractive index increases with increasing applied bias voltage above −140 V.[38] However, PIAD SiO_2 films with a higher refractive index (1.47) also have an oxygen deficiency leading to increased optical losses when the films are deposited at an average-bias voltage above a threshold value (around −150 V, using Ar^+ as bombarding ions). Hence, the optimization of the process parameters is a key responsibility to achieve desired properties.

For the PEALD process performed in the SILAYO tool, the gas mixture during the plasma pulse consists mainly of O_2 gas with *ca.* 15% Ar, unlike the gas used in the FlexAL tool which consists of pure O_2. Hence, both chemically reactive oxygen ions and chemically inert argon ions are available to enhance the surface reactions for the PEALD process in the SILAYO tool. This can play a role in the differences observed for the properties of SiO_2 films grown in the two reactors. Differences in the deposition temperature might also affect the properties. The SiO_2 thin films obtained by PEALD processes with substrate biasing simultaneously have a higher refractive index (1.47 at 633 nm) and lower optical losses than PIAD layers. The PEALD SiO_2 coatings grown with substrate biasing (−295 V using the FlexAL tool and −1 V using the SILAYO tool) have a refractive index similar to that of films grown by the IBSD method with Ar^+ ion bombardment; however, the refractive

Published on 19 December 2019. Downloaded by Eindhoven University of Technology on 2/12/2020 12:29:42 PM.

index remains slightly lower than that obtained by IBSD with Xe gas. Hence, systematic and thorough studies are necessary to investigate the effect of various gases and composition in PEALD processes assisted by ions.

Optical losses in the films deposited on fused silica and BK7 substrates using the FlexAL tool were determined by spectrophotometry. Optical losses in the films can arise from absorption and scattering. Scattering losses are probably minimal for these films since XRD data (not shown) have indicated completely amorphous films and the smooth surface is confirmed by AFM measurements (Fig. 3).

Optical losses (OL) corresponding to the sum of scattering and absorption losses are determined from transmittance and reflectance measurements at near normal angle of incidence as OL = $1 - T - R$. Fig. 9 shows higher optical losses (in the UV range) in SiO_2 film deposited without than with substrate biasing on fused silica substrates using the FlexAL tool. The high optical losses in the film deposited without substrate biasing can be due to impurities present in film or absorption due to oxygen deficiency (SiO_x, $x < 2$)[38] as shown in Table 5.

Deposition mechanism

Fig. 10 shows possible elementary surface reactions for the PEALD process using BDEAS precursor reacting with –OH groups on the hydroxylated SiO_2 surface. The reactions 1 and 2a lead to products **P1** and **P2** with the organic precursor connected to one or two surface oxygen atoms, respectively. **P1** converts to **P2** by reaction 2b. After the second half-cycle (plasma pulse), **P1** and **P2** are fully oxidized to **S1** and **S2** featuring a new surface Si atom with three or two –OH groups, respectively. Reaction 3 converts **S1** to **S2** by releasing H_2O. We focused on elementary reactions 1, 2a, 2b and 3 because it was shown that bonds between the precursor Si atom and the surface are not altered by oxygen radical species.[93]

Energetics of surface reactions

Energetics of all elementary reactions 1, 2a, 2b, and 3 have been investigated previously[59] using DFT and two cluster

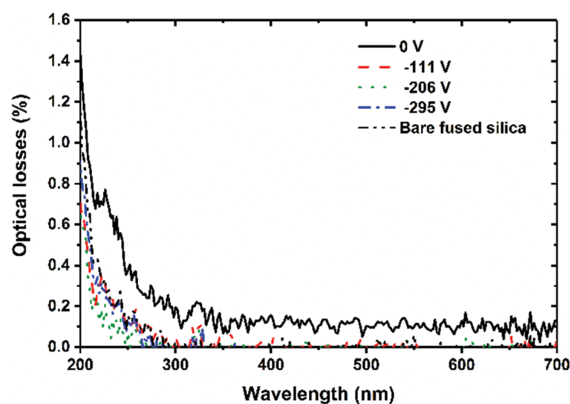

Fig. 9 The optical losses of SiO_2 films (using the FlexAL tool) deposited on fused silica substrate with different average-bias voltages.

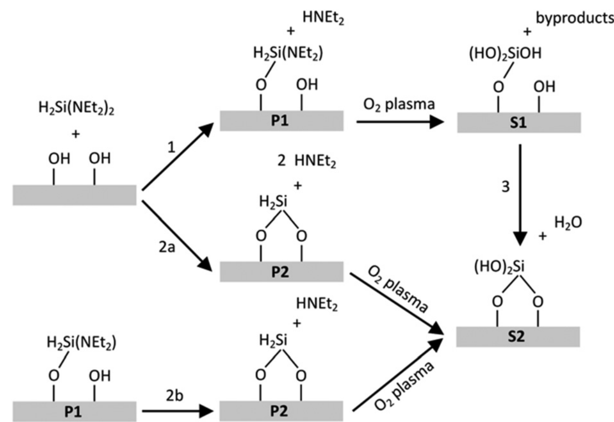

Fig. 10 Elementary surface reactions during PEALD deposition of SiO_2 film using BDEAS precursor. **P1** and **P2** are products of the precursor deposition. **S1** and **S2** are products of the plasma pulse.

models of two neighbouring –OH groups without surface constraints as well as a two-dimensional (2D) periodic hydroxylated α-quartz (0001) surface. For the small, flexible cluster model, the reaction energies ΔE_r of reactions 1, 2a, 2b, and 3 are −58.3, −64.3, −6.0 kJ mol^{-1}, and +37.5 kJ mol^{-1}, respectively. For the more rigid cage cluster the respective reaction energies are −67.0, −30.5, +36.5, and +63.0 kJ mol^{-1}. For the 2D surface model, the respective reaction energies are −63.0, −18.4, +44.6, and +60.9 kJ mol^{-1}. The energy of reaction 1 involving only one surface –OH group is similar for all three models. Reaction 2a is exothermic, but its reaction energies increase with rigidity of the model. In contrast, reaction energies for 2b and 3 involving conversions of **P1** to **P2** and **S1** to **S2**, respectively, are significantly lower. This points to an important role of surface constraints, since bringing two surface oxygen atoms close enough to create **P2** and **S2** is connected with energy penalty.

PEALD thin film properties are expected to change due to accelerated ions by electric field during the plasma step. However, to fully exclude the possibility that the electric field itself affects the surface chemistry we have investigated the direct effect of applied field on the structure and stabilities of **S1** and **S2** on the 2D surface model. This was achieved by DFT structure optimizations with the explicit application of a uniform electric field perpendicular to the surface. For both **S1** and **S2**, the energy is influenced by less than 6.5 kJ mol^{-1} for even very high field strengths up to 1.0 V nm^{-1}. Virtually no effect was found on atomic structures when optimized under the influence of the electric field.

However, the applied electric field can influence the properties of PEALD deposited films by energy transfer between the plasma sheath and the surface due to acceleration of the bombarding ions. For ions of low energy (in the range of 100 eV), like in PEALD, the majority of the ions cannot penetrate the repulsive potential barrier of the surface and are deflected.[71] However, a substantial part of the ion energy is transferred to lattice vibrations of surface atoms close to the

This journal is © The Royal Society of Chemistry 2020

Published on 19 December 2019. Downloaded by Eindhoven University of Technology on 2/12/2020 12:29:42 PM.

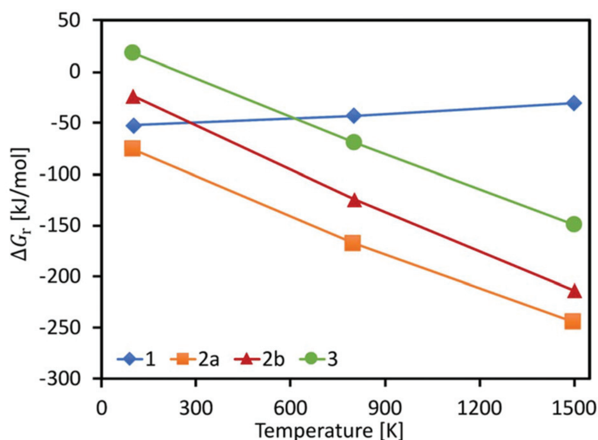

Fig. 11 Gibbs free reaction energies ΔG_r of elementary reactions 1, 2a, 2b and 3 as a function of temperature for the small cluster model of hydroxylated SiO_2 surface.

impact point. This effectively raises the local temperature in this region of the material to values sufficiently high to alter surface reactions.[71,94] In order to estimate the effect of these so-called thermal spikes on the SiO_2 deposition process we have calculated Gibbs free reaction energies ΔG_r for reactions 1, 2a, 2b, and 3 as a function of temperature, shown in Fig. 11. In the case of reaction 1, ΔG_r increases slightly with increasing temperature. In contrast, ΔG_r of reactions 2a, 2b and 3 strongly decreases with increasing temperature. This is an expected result since the number of gaseous products remains unchanged for reaction 1 but increases for reactions 2a, 2b and 3. It implies a larger entropy change ΔS for reactions 2a, 2b and 3 compared to reaction 1 and a stronger temperature dependence of ΔG_r due to the $-T\Delta S$ term. Therefore, thermal spikes at the surface caused by ion bombardment would clearly favour the creation of **S2** surface species by reactions 2b and 3. Note, that the thermal spikes are very localized and, therefore, not equivalent to uniform heating of the whole substrate, which could cause other effects such as desorption of the precursor. Since even very low average-bias values are sufficient to alter the growth of silica thin films in PEALD processes, the proton transfer process involved in reactions 2b and 3 seem to be activated by the low energy ions.

Direct PEALD simulations

The localized thermal spikes at the surface due to an ion bombardment increase the number of **S2** surface species present after the plasma pulse by lowering ΔG_r for the reactions 2b and 3. Our PEALD simulation protocol[59] accounts for the temperature dependence of ΔG_r in a simplified way using a predefined probability p_{P2} for creation of **P2** (precursor bonded to two surface O atoms) at each deposition step. The probability for creation of **P1** (precursor bonded to one surface O atom) is $p_{P1} = 1 - p_{P2}$. As evident from Fig. 12 these probabilities have a significant impact on the structure of PEALD layers. Increasing p_{P2} favours the densification of growing SiO_2 layers, whereas decreasing p_{P2} results in amorphous film growth and void formation.[59] For $p_{P2} = 0$ each BDEAS molecule reacts with only one surface –OH group yielding **P1**. After the plasma pulse, **P1** is converted to **S1** containing deposited Si atoms with three –OH groups. Therefore, the number of hydroxyl groups increases compared to the initial state. This leads to an amorphous growth of the deposited film, creation of voids and OH impurities. In contrast, for $p_{P2} = 1$ the maximum possible number of **P2** sites is created after the first half-cycle. The plasma pulse converts them to **S2** containing deposited Si atom with two –OH groups and the number of hydroxyl groups remains unchanged compared to the initial surface state. In combination with the formation of compact Si–O–Si bridges this results in a dense film.

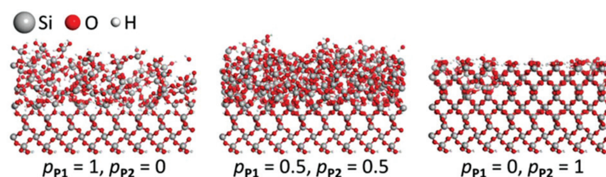

Fig. 12 Simulated structures of PEALD deposited SiO_2 with different probabilities p_{P1} and p_{P2}.[59]

The film morphology of the layers grown without electric field corresponds to reactions governed by **P1** with a more porous structure. In contrast, applying an electric field in the PEALD process allows alteration of the surface reactions leading to a **P2** dominated film structure. A significant reduction of the amount of hydroxyl groups trapped within the SiO_2 layer is experimentally observed by FTIR spectra of silica films grown under an external electric field. As shown in Fig. 6b and d the characteristic Si–OH peak at 3386 cm^{-1} corresponding to OH stretching vibrational modes of –OH groups, which are involved in intra or intermolecular hydrogen bonds, is virtually absent in silica films deposited already at an average-bias voltage of −111 V with the FlexAL and −1 V with the SILAYO tool. This result is fully consistent with our simulations. The increased number of **S2** surface sites after each plasma pulse caused by temperature spikes due to ion bombardment under electric field results in a smaller amount of the –OH groups trapped in the SiO_2 layer. This effect is clearly visible in Fig. 12 when comparing SiO_2 structures grown for $p_{P2} = 0$ and $p_{P2} = 0.5$ with the one obtained for $p_{P2} = 1$.

Conclusion

The effect of energetic ions on the growth, composition and material properties of SiO_2 thin films deposited by PEALD were thoroughly investigated. Two different reactor configurations have been applied for the growth of the films, and a similar trend is observed when a bias is applied during the plasma pulse in both tools. Already at very low average-bias voltage values, there is a pronounced change in the material properties and growth behaviour. Applying an electric field has

View Article Online

Published on 19 December 2019. Downloaded by Eindhoven University of Technology on 2/12/2020 12:29:42 PM.

no significant influence on the surface morphology. However, it results in denser films with nearly no open pores, low optical losses, control over the mechanical stress, and more stoichiometric films than without a bias. The refractive index of the PEALD SiO_2 layer grown with an electric field is comparable with the refractive index of PIAD and IBSD coatings. The experimental findings are supported by density functional theory and atomistic simulations. The simulations and theoretical considerations demonstrate that the application of an external electric field during the plasma step results in an increased energy transfer between the accelerated ions in the plasma sheath and the surface, directly influencing the relevant surface reactions. In particular, thermal spikes at the surface caused by ion bombardment result in a higher probability for precursor binding to two surface oxygen atoms. This leads to dense SiO_2 films, increased amount of Si–O–Si bridges and a reduction of OH impurities. Hence, this technique is a robust method towards improving the SiO_2 film properties by increasing density and refractive index and reducing open pores in the film for various applications.

Conflicts of interest

There are no conflicts to declare.

Acknowledgements

Funding by the Deutsche Forschungsgemeinschaft (DFG, German Research Foundation) – Priority Programme Fields Matter 1959/1 within the projects SZ253/2-1 and SI938/8-1 and by the Fraunhofer Society within the Attract 066-601020 project is gratefully acknowledged.

References

1 S. Eränen, in *Handbook of Silicon Based MEMS Materials and Technologies*, ed. V. Lindroos, M. Tilli, A. Lehto and T. Motooka, William Andrew Publishing, Boston, 2010, ch. 8, pp. 137–148.

2 J. Foggiato, in *Handbook of Thin Film Deposition Processes and Techniques*, ed. K. Seshan, William Andrew Publishing, Norwich, NY, 2nd edn, 2001, ch. 3, pp. 111–150.

3 L. Martinu and D. Poitras, *J. Vac. Sci. Technol., A*, 2000, **18**, 2619–2645.

4 N. Kaiser and H. K. Pulker, *Optical interference coatings*, 2003.

5 U. Schulz, U. B. Schallenberg and N. Kaiser, *Appl. Opt.*, 2002, **41**, 3107–3110.

6 M. L. Grilli, F. Menchini, A. Piegari, D. Alderighi, G. Toci and M. Vannini, *Thin Solid Films*, 2009, **517**, 1731–1735.

7 J. P. Dai, W. Gao, B. Liu, X. L. Cao, T. Tao, Z. L. Xie, H. Zhao, D. J. Chen, H. Ping and R. Zhang, *Appl. Surf. Sci.*, 2016, **364**, 886–891.

8 V. Zhupanov, I. Kozlov, V. Fedoseev, P. Konotopov, M. Trubetskov and A. Tikhonravov, *Appl. Opt.*, 2017, **56**, C30–C34.

9 K. Pfeiffer, L. Ghazaryan, U. Schulz and A. Szeghalmi, *ACS Appl. Mater. Interfaces*, 2019, **11**, 21887–21894.

10 S. W. Glunz and F. Feldmann, *Sol. Energy Mater. Sol. Cells*, 2018, **185**, 260–269.

11 J. Schmidt, R. Peibst and R. Brendel, *Sol. Energy Mater. Sol. Cells*, 2018, **187**, 39–54.

12 V. Cremers, R. L. Puurunen and J. Dendooven, *Appl. Phys. Rev.*, 2019, **6**, 021302.

13 A. Pakkala and M. Putkonen, in *Handbook of Deposition Technologies for Films and Coatings*, ed. P. M. Martin, William Andrew Publishing, Boston, 3rd edn, 2010, pp. 364–391.

14 J. Dendooven, D. Deduytsche, J. Musschoot, R. L. Vanmeirhaeghe and C. Detavernier, *J. Electrochem. Soc.*, 2009, **156**, P63–P67.

15 J. W. Elam, D. Routkevitch, P. P. Mardilovich and S. M. George, *Chem. Mater.*, 2003, **15**, 3507–3517.

16 K. Pfeiffer, U. Schulz, A. Tünnermann and A. Szeghalmi, *Coatings*, 2017, **7**, 118.

17 H. B. Profijt, S. E. Potts, M. C. M. van de Sanden and W. M. M. Kessels, *J. Vac. Sci. Technol., A*, 2011, **29**, 050801.

18 S. E. Potts, H. B. Profijt, R. Roelofs and W. M. M. Kessels, *Chem. Vap. Deposition*, 2013, **19**, 125–133.

19 S. E. Potts and W. M. M. Kessels, *Coord. Chem. Rev.*, 2013, **257**, 3254–3270.

20 G. Dingemans, C. A. A. van Helvoirt, D. Pierreux, W. Keuning and W. M. M. Kessels, *J. Electrochem. Soc.*, 2012, **159**, H277–H285.

21 H. B. Profijt, M. C. M. van de Sanden and W. M. M. Kessels, *Electrochem. Solid-State Lett.*, 2012, **15**, G1–G3.

22 H. B. Profijt, M. C. M. van de Sanden and W. M. M. Kessele, *J. Vac. Sci. Technol., A*, 2013, **31**, 01A106.

23 S. Ratzsch, E. B. Kley, A. Tünnermann and A. Szeghalmi, *Materials*, 2015, **8**, 7805–7812.

24 T. Faraz, H. C. M. Knoops, M. A. Verheijen, C. A. A. van Helvoirt, S. Karwal, A. Sharma, V. Beladiya, A. Szeghalmi, D. M. Hausmann, J. Henri, M. Creatore and W. M. M. Kessels, *ACS Appl. Mater. Interfaces*, 2018, **10**, 13158–13180.

25 T. Faraz, K. Arts, S. Karwal, H. C. M. Knoops and W. M. M. Kessels, *Plasma Sources Sci. Technol.*, 2019, **28**, 024002.

26 V. Beladiya, T. Faraz, W. M. M. Kessels, A. Tünnermann and A. Szeghalmi, *Proc. SPIE*, 2018, **10691**, 106910e.

27 D. M. Mattox, in *Handbook of Physical Vapor Deposition (PVD) Processing*, ed. D. M. Mattox, William Andrew Publishing, Boston, 2nd edn, 2010, ch. 7, pp. 237–286.

28 S. G. Walton and J. E. Greene, in *Handbook of Deposition Technologies for Films and Coatings*, ed. P. M. Martin, William Andrew Publishing, Boston, 3rd edn, 2010, ch. 2, pp. 32–92.

29 R. Gago, I. Jiménez and J. M. Albella, in *Materials Surface Processing by Directed Energy Techniques*, ed. Y. Pauleau, Elsevier, Oxford, 2006, ch. 10, pp. 345–382.

30 T. Takagi, *J. Vac. Sci. Technol., A*, 1984, **2**, 382–388.

This journal is © The Royal Society of Chemistry 2020

Published on 19 December 2019. Downloaded by Eindhoven University of Technology on 2/12/2020 12:29:42 PM.

31 H. K. Pulker, *Surf. Coat. Technol.*, 1999, **112**, 250–256.
32 D. Manova, J. W. Gerlach and S. Mandl, *Materials*, 2010, **3**, 4109–4141.
33 S. M. Rossnagel, J. J. Cuomo and W. D. Westwood, *Handbook of plasma processing technology : fundamentals, etching, deposition, and surface interactions*, Noyes Publications, Park Ridge, N.J., U.S.A., 1990.
34 D. M. Mattox, *J. Vac. Sci. Technol., A*, 1989, **7**, 1105–1114.
35 J. J. Cuomo and S. M. Rossnagel, *Nucl. Instrum. Methods Phys. Res.*, 1987, **19–20**, 963–974.
36 S. M. Rossnagel and J. J. Cuomo, *Thin Solid Films*, 1989, **171**, 143–156.
37 A. Anders, *Thin Solid Films*, 2010, **518**, 4087–4090.
38 R. Thielsch, A. Gatto, J. Heber and N. Kaiser, *Thin Solid Films*, 2002, **410**, 86–93.
39 D. A. Carl, D. W. Hess, M. A. Lieberman, T. D. Nguyen and R. Gronsky, *J. Appl. Phys.*, 1991, **70**, 3301–3313.
40 A. J. Waldorf, J. A. Dobrowolski, B. T. Sullivan and L. M. Plante, *Appl. Opt.*, 1993, **32**, 5583–5593.
41 R. G. Andosca, W. J. Varhue and E. Adams, *J. Appl. Phys.*, 1992, **72**, 1126–1132.
42 L. Zajícková, J. Janca and V. Perina, *Thin Solid Films*, 1999, **338**, 49–59.
43 N. Benissad, K. Aumaille, A. Granier and A. Goullet, *Thin Solid Films*, 2001, **384**, 230–235.
44 S. B. Bang, T. H. Chung and Y. Kim, *Thin Solid Films*, 2003, **444**, 125–131.
45 S. B. Bang, T. H. Chung, Y. Kim, M. S. Kang and J. K. Kim, *J. Phys. D: Appl. Phys.*, 2004, **37**, 1679–1684.
46 D. Goghero, A. Goullet and J. P. Landesman, *Solid-State Electron.*, 2005, **49**, 369–376.
47 C. H. Jeong, J. H. Lee, J. T. Lim, N. G. Cho, C. H. Moon and G. Y. Yeom, *Jpn. J. Appl. Phys., Part 1*, 2005, **44**, 1022–1026.
48 L. N. He and S. Hasegawa, *Jpn. J. Appl. Phys., Part 1*, 2001, **40**, 4672–4676.
49 N. Jiang, B. Agius, M. C. Hugon, J. Olivier and M. Puech, *J. Appl. Phys.*, 1994, **76**, 1847–1855.
50 K. Pfeiffer, S. Shestaeva, A. Bingel, P. Munzert, L. Ghazaryan, C. van Helvoirt, W. M. M. Kessels, U. T. Sanli, C. Grevent, G. Schütz, M. Putkonen, I. Buchanan, L. Jensen, D. Ristau, A. Tünnermann and A. Szeghalmi, *Opt. Mater. Express*, 2016, **6**, 660–670.
51 M. Putkonen, M. Bosund, O. M. E. Ylivaara, R. L. Puurunen, L. Kilpi, H. Ronkainen, S. Sintonen, S. Ali, H. Lipsanen, X. W. Liu, E. Haimi, S. P. Hannula, T. Sajavaara, I. Buchanan, E. Karwacki and M. Vähä-Nissi, *Thin Solid Films*, 2014, **558**, 93–98.
52 M. C. Schwille, T. Schössler, F. Schön, M. Oettel and J. W. Bartha, *J. Vac. Sci. Technol., A*, 2017, **35**, 01B119.
53 R. Ahlrichs, M. Bär, M. Häser, H. Horn and C. Kölmel, *Chem. Phys. Lett.*, 1989, **162**, 165–169.
54 F. Furche, R. Ahlrichs, C. Hättig, W. Klopper, M. Sierka and F. Weigend, *Wiley Interdiscip. Rev.: Comput. Mol. Sci.*, 2014, **4**, 91–100.
55 J. P. Perdew, K. Burke and M. Ernzerhof, *Phys. Rev. Lett.*, 1996, **77**, 3865–3868.
56 F. Weigend and R. Ahlrichs, *Phys. Chem. Chem. Phys.*, 2005, **7**, 3297–3305.
57 S. Grimme, J. Antony, S. Ehrlich and H. Krieg, *J. Chem. Phys.*, 2010, **132**, 154104.
58 S. Grimme, S. Ehrlich and L. Goerigk, *J. Comput. Chem.*, 2011, **32**, 1456–1465.
59 M. Becker and M. Sierka, *Materials*, 2019, **12**, 2605.
60 A. H. Larsen, J. J. Mortensen, J. Blomqvist, I. E. Castelli, R. Christensen, M. Dulak, J. Friis, M. N. Groves, B. Hammer, C. Hargus, E. D. Hermes, P. C. Jennings, P. B. Jensen, J. Kermode, J. R. Kitchin, E. L. Kolsbjerg, J. Kubal, K. Kaasbjerg, S. Lysgaard, J. B. Maronsson, T. Maxson, T. Olsen, L. Pastewka, A. Peterson, C. Rostgaard, J. Schiotz, O. Schütt, M. Strange, K. S. Thygesen, T. Vegge, L. Vilhelmsen, M. Walter, Z. H. Zeng and K. W. Jacobsen, *J. Phys.: Condens. Matter*, 2017, **29**, 273002.
61 J. D. Gale and A. L. Rohl, *Mol. Simul.*, 2003, **29**, 291–341.
62 A. C. T. van Duin, S. Dasgupta, F. Lorant and W. A. Goddard, *J. Phys. Chem. A*, 2001, **105**, 9396–9409.
63 R. M. Abolfath, A. C. T. van Duin and T. Brabec, *J. Phys. Chem. A*, 2011, **115**, 11045–11049.
64 O. Rahaman, A. C. T. van Duin, W. A. Goddard and D. J. Doren, *J. Phys. Chem. B*, 2011, **115**, 249–261.
65 H. Jung, W. H. Kim, I. K. Oh, C. W. Lee, C. Lansalot-Matras, S. J. Lee, J. M. Myoung, H. B. R. Lee and H. Kim, *J. Mater. Sci.*, 2016, **51**, 5082–5091.
66 S. Shestaeva, A. Bingel, P. Munzert, L. Ghazaryan, C. Patzig, A. Tünnermann and A. Szeghalmi, *Appl. Opt.*, 2017, **56**, C47–C59.
67 A. Lefevre, L. J. Lewis, L. Martinu and M. R. Wertheimer, *Phys. Rev. B*, 2001, **64**, 115429.
68 D. Choi, B. K. Kim, K. B. Chung and J. S. Park, *Mater. Res. Bull.*, 2012, **47**, 3004–3007.
69 D. Hausmann, J. Becker, S. L. Wang and R. G. Gordon, *Science*, 2002, **298**, 402–406.
70 M. Koster and H. M. Urbassek, *Phys. Rev. B: Condens. Matter Mater. Phys.*, 2001, **63**, 224111.
71 G. Carter, *J. Phys. D: Appl. Phys.*, 1994, **27**, 1046–1055.
72 H. P. Ma, J. H. Yang, J. G. Yang, L. Y. Zhu, W. Huang, G. J. Yuan, J. J. Feng, T. C. Jen and H. L. Lu, *Nanomaterials*, 2019, **9**, 55.
73 P. G. Pai, S. S. Chao, Y. Takagi and G. Lucovsky, *J. Vac. Sci. Technol., A*, 1986, **4**, 689–694.
74 M. Vishwas, K. N. Rao, A. R. Phani, K. V. A. Gowda and R. P. S. Chakradhar, *Spectrochim. Acta, Part A*, 2011, **78**, 695–699.
75 S. H. Jeong, J. K. Kim, B. S. Kim, S. H. Shim and B. T. Lee, *Vacuum*, 2004, **76**, 507–515.
76 C. Régnier, P. Tristant and J. Desmaison, *Surf. Coat. Technol.*, 1996, **80**, 18–22.
77 L. Ghazaryan, E. B. Kley, A. Tünnermann and A. Szeghalmi, *Nanotechnology*, 2016, **27**, 255603.
78 L. Ghazaryan, E. B. Kley, A. Tünnermann and A. V. Szeghalmi, *J. Vac. Sci. Technol., A*, 2013, **31**, 01A149.
79 H. Seidel, L. Csepregi, A. Heuberger and H. Baumgärtel, *J. Electrochem. Soc.*, 1990, **137**, 3612–3626.

Published on 19 December 2019. Downloaded by Eindhoven University of Technology on 2/12/2020 12:29:42 PM.

80 V. Bhatt and S. Chandra, *J. Micromech. Microeng.*, 2007, **17**, 1066–1077.
81 L. Simurka, R. Ctvrtlík, J. Tomastik, G. Bektas, J. Svoboda and K. Bange, *Chem. Pap.*, 2018, **72**, 2143–2151.
82 G. N. Straus, in *Optical Interference Coatings*, ed. H. K. P. Norbert Kaiser, Springer, Berlin, Heidelberg, Berlin, 2003, vol. 88, pp. 207–229.
83 G. Knuyt, W. Lauwerens and L. M. Stals, *Thin Solid Films*, 2000, **370**, 232–237.
84 D. J. Ward and R. D. Arnell, *Thin Solid Films*, 2002, **420–421**, 269–274.
85 I. Petrov, P. B. Barna, L. Hultman and J. E. Greene, *J. Vac. Sci. Technol., A*, 2003, **21**, S117–S128.
86 E. Chason and P. R. Guduru, *J. Appl. Phys.*, 2016, **119**, 191101.
87 E. Chason, M. Karlson, J. J. Colin, D. Magnfält, K. Sarakinos and G. Abadias, *J. Appl. Phys.*, 2016, **119**, 145307.
88 G. Abadias, E. Chason, J. Keckes, M. Sebastiani, G. B. Thompson, E. Barthel, G. L. Doll, C. E. Murray, C. H. Stoessel and L. Martinu, *J. Vac. Sci. Technol., A*, 2018, **36**, 020801.
89 Z. Zhu, P. Sippola, O. M. E. Ylivaara, C. Modanese, M. Di Sabatino, K. Mizohata, S. Merdes, H. Lipsanen and H. Savin, *Nanoscale Res. Lett.*, 2019, **14**, 55.
90 A. Szekeres and P. Danesh, *Semicond. Sci. Technol.*, 1996, **11**, 1225–1230.
91 Y. S. Lee, J. H. Han, J. S. Park and J. Park, *J. Vac. Sci. Technol., A*, 2017, **35**, 041508.
92 M. Mateev, T. Lautenschläger, D. Spemann, A. Finzel, J. W. Gerlach, F. Frost and C. Bundesmann, *Eur. Phys. J. B*, 2018, **91**, 45.
93 G. Y. Fang, L. N. Xu, Y. Q. Cao, L. G. Wang, D. Wu and A. D. Li, *Chem. Commun.*, 2015, **51**, 1341–1344.
94 E. H. Hirsch and I. K. Varga, *Thin Solid Films*, 1980, **69**, 99–105.

This journal is © The Royal Society of Chemistry 2020